How are the equivalent damping ratios modified by nonlinear engineering demand parameters?

Thomas Heitz, Cédric Giry, Benjamin Richard, Frédéric Ragueneau

COMPDYN 2017
6th ECCOMAS Thematic Conference on
Computational Methods in Structural Dynamics and Earthquake Engineering
M. Papadrakakis, M. Fragiadakis (eds.)
Rhodes Island, Greece, 15–17 June, 2017

HOW ARE THE EQUIVALENT DAMPING RATIOS MODIFIED BY NONLINEAR ENGINEERING DEMAND PARAMETERS?

Thomas Heitz[1,2], **Cédric Giry**[1], **Benjamin Richard**[2], **Frédéric Ragueneau** [1]

[1]LMT-Cachan,
CNRS/Paris-Saclay University,
61 avenue du Président Wilson, F-94230, Cachan, France.
e-mail: {heitz,giry,ragueneau}@lmt.ens-cachan.fr

[2]Den-Service d'études mécaniques et thermiques (SEMT), CEA, Université Paris-Saclay,
F-91191, Gif-sur-Yvette, France.
e-mail: benjamin.richard@cea.fr

Keywords: Dissipations, Reinforced concrete, Viscous damping, Experiments, Model identification, TAMARIS

Abstract. *When attempting to predict the seismic response of reinforced concrete (RC) structures, a trade-off has to be found out between a realistic representation of the dissipations through material behavior law and a numerically more efficient modeling with a controlled computational demand such as a Rayleigh-type damping model. Anyway, constitutive laws only describe internal dissipation and actually need a complementary dissipation term often chosen as a proportional damping matrix to take into account external dissipation sources such as interactions with the environment. Decoupling these two contributions in global dissipation measurement from experimental tests is still challenging. To address this problem, a numerical study based on an experimentally identified structural model is here presented. To this end, an experimental campaign has been carried out on RC beams set up on the AZALEE shaking table of the TAMARIS experimental facility operated by the French Alternative Energies and Atomic Energy Commission (CEA). In this paper, the experimental campaign is first presented. Secondly, a suited constitutive model is formulated and identified from the experimental results. Third, numerical dynamic experiments are carried out in order to assess the influence of several parameters on the energy dissipation and on the equivalent viscous damping ratio through two different methods. The validity of these results is assessed on a numerical case where a nonlinear model and an equivalent linear model are compared with each other. Experimental results of dynamic tests are also used as reference in order to estimate the additional viscous damping necessary to take into account the whole energy dissipation.*

1 INTRODUCTION

Despite the increasing accuracy of models for nonlinear behavior of RC structures, their combination with complex finite element (FE) meshes still leads to high computational cost. In practice, an additional viscous damping is often used to account for dissipations not taken into account by the structural model [1, 2], particularly in its linear domain [3]. As shown in [4, 5], combining both types of dissipations (i.e. hysteretic and viscous damping) can compromise the validity of a study and could require a reduction of the viscous damping in the nonlinear range [3]. In order to represent this dependency, several evolving Rayleigh-type viscous damping models have been proposed (see [6] for a study of such models), but experimental evidences on slender buildings tend to show that modal viscous damping can be thought to be an intermediate between constant viscous damping for all modes and stiffness-proportional damping [7, 8]. Before performing such a fine analysis, simplified methodologies should be used in order to obtain a first design of a structure. Displacement-based methods have became popular for the past decades, but they generally require the knowledge of a monotonous force-displacement curve and the value of an equivalent viscous damping. This damping ratio has a key role when assessing maximum structural responses and some studies show it is the second source of uncertainties after the ground motions [9, 10]. Nevertheless, this assumed equivalence with the energy dissipated hysteretically may be questionable. Indeed, the identification is performed on quasi-static loadings whereas damping ratio is used for seismic loadings. In addition, several studies have emphasized the fact that the viscous damping depends on the response amplitude for RC buildings [11, 12, 8], which contradicts the hypothesis of a *linear* equivalent viscous damping. To verify if the previous observations made on buildings comply with RC components, beams in the present study, and evaluate the influence of different excitation and material parameters, an experimental campaign described in the following section has been carried out and is followed by numerical experiments calibrated on experimental data.

2 EXPERIMENTAL CAMPAIGN

2.1 Motivations

An experimental campaign has been set up on RC beams by means of the AZALEE shaking table, as part of the TAMARIS experimental facility operated by the French Alternative Energies and Atomic Energy Commission (CEA) [13]. The main objective was to provide reference data through both dynamic and quasistatic tests in order to evaluate the dissipations depending on structural, material and signal characteristics. The measure of damping forces is challenging because their levels are unknown and generally more difficult to investigate than acceleration or restoring forces [14], they exhibit several sources and evolve along the time-history analysis. In order to quantify and to analyze the dissipation and its evolution during quasi-static and dynamic loadings, a dense network of svarious sensors type have been mounted on the experimental setup. Furthermore, an important design effort was made on the technological choices for the samples and the boundary conditions. This section describes briefly a part of the experimental campaign setup which is necessary to provide the data used in this work. For a more extensive description, please refer to [15].

2.2 RC Specimens

A RC beams have been chosen as specimens because they are widespread structural elements and a large choice of more or less simple models are available in the literature, depending on the

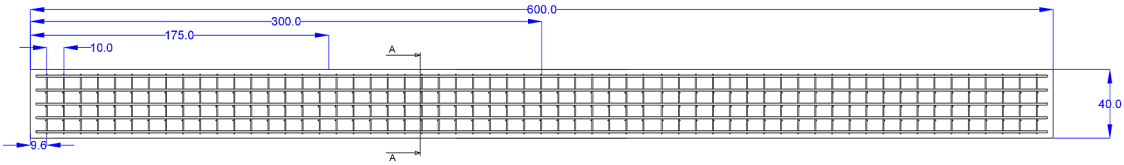

(a) Longitudinal reinforcements

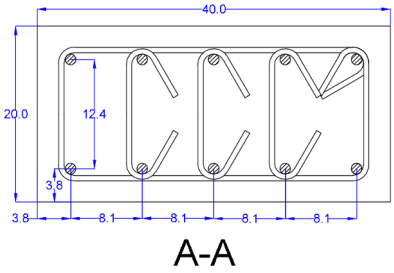

(b) Cross-section reinforcements

Figure 1: 10HA12 RC beam reinforcements

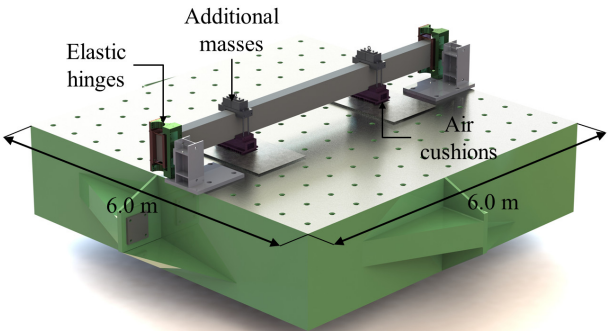

Figure 2: General view of the experimental setup.

description refinement. Different variations of the reference design have been made in order to explore the influence of material and structural parameters. The beam considered in the present study is referred as 10HA12-C1B, standing for 10 12mm-diameter steel reinforcement bars in the section of the beam, for a concrete of $29.7\,\mathrm{MPa}$ strength and $28.1\,\mathrm{GPa}$ Young's modulus. The steel reinforcement pattern is given in figures 1a and 1b.

2.3 Setup

To better understand and visualize the items described in the following subsections, a general view of the final experimental setup is presented in figure 2. Elastic hinges based upon high performance steel blades are used at both ends to link the beam with the shaking table or the strong floor. The blades have been designed to be the less stiff as possible so that they deform elastically all along the tests, avoiding by this way the dissipations due to friction or assembly plays. The beam weight is supported by air pads allowing to drastically reduce the friction forces between the beam and the floor during the bending. Indeed, bearing the vertical forces through the extremal supports would have induced bending cracks because of the 6 meters span.

In accordance with the frequency band of the shaking table (i.e. frequency band with a robust

online control), the two first eigenfrequencies of the structure are kept below $30\,\mathrm{Hz}$. This choice leads to a strong design criterion. In addition, a highly damaged state of the beam should be reached in order to quantify the influence of damage on the damping properties. This design constraint has also been tackled by the use of two additional masses of $360\,\mathrm{kg}$ each tighten to the specimen, bringing the total moving mass (the beam plus the additional masses) to $1870\,\mathrm{kg}$.

3 OVERVIEW OF EXISTING EQUIVALENT VISCOUS DAMPING IDENTIFICATION PROCEDURES

3.1 Energy balance in the expression of the viscous damping ratio

Considering an ideal system, the expression of the viscous damping ratio will be here below. The notations are defined in figure 3.

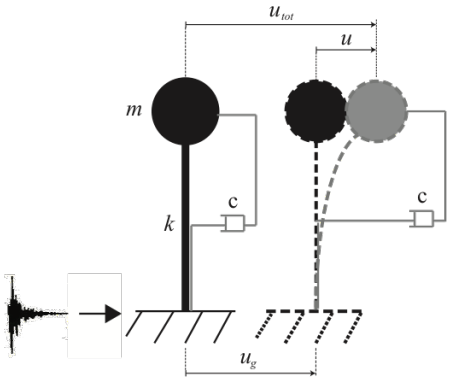

Figure 3: Notations used for the considered mass-spring-damper oscillating system

If the ground motion is an harmonic acceleration $\ddot{u}_g = -U_g\omega^2\cos(\omega t)$, the steady state displacement and velocity will be given by equations 1 and 2 where U is the response displacement amplitude, ω is the excitation pulsation and Φ is the phase angle.

$$u(t) = U\cos(\omega t - \Phi) \tag{1}$$

$$\dot{u}(t) = -U\omega\sin(\omega t - \Phi) \tag{2}$$

The corresponding energy dissipated during one cycle by the damper is E_d expressed in equation 4 with ω_0 the natural pulsation of the system.

$$E_d = \oint F_D.du = \oint c\dot{u}^2dt = \int_0^{\frac{2\pi}{\omega}} c\,U^2\omega^2\sin(\omega t - \Phi)^2dt \; = \pi c\omega U^2 = 2\pi\xi\omega\omega_0 mU^2 \tag{3}$$

$$E_d = 2\pi\xi\frac{\omega}{\omega_0}kU^2 \tag{4}$$

For a purely linear spring, the maximum stored elastic energy is:

$$E_s = \int_0^U ku\cdot du = \frac{1}{2}kU^2 \tag{5}$$

Thus, from equations 4 and 5, one can define the viscous damping ratio as:

$$\xi = \frac{1}{4\pi}\frac{\omega_0}{\omega}\frac{E_d}{E_s} \tag{6}$$

At this point, it is clear that the viscous damping ratio of a linear oscillator depends not only on the ratio between de dissipated energy over the maximum stored energy, but also on the ratio between the natural pulsation of the oscillator and the excitation pulsation.

3.2 Jacobsen's areas method

The first option to evaluate an equivalent viscous damping ratio by an energy equivalence approach to estimate hysteretic dissipations has been made by [16, 17]. The method was originally developed to evaluate the equivalent viscous damping ratio (EVDR) for nonlinear frictional system. Several points remain questionable:

- to overcome the frequency dependency and to ensure the loops continuity, it is assumed that the excitation is harmonic with the same frequency as the natural frequency of the system (see equation 6 with $\omega = \omega_0$). However, it is a common practice to perform a quasi-static cyclic test on the hysteretic damper to evaluate the associated EVDR;
- while the energy dissipated by a linear viscous damper is linearly proportional with respect to the excitation frequency (see equation 4), the energy dissipated by the hysteretic damper to be approximated is not. Hence, for any excitation with a frequency content higher than the oscillator's natural frequency, the viscous damping ratio will be overestimated and *vice-versa*;
- the stored energy is generally supposed to be square-proportional to the displacement (figure 4a) but this hypothesis is inexact in the case of a nonlinear behavior which is the case when pinching occurs for example (figure 4b);
- when the loops are not symmetric, there is no actual reason to pick up the maximum relative displacement rather than the minimum one when assessing the stored elastic energy. For this reason, [18] proposed an approach adapted to asymmetric hysteretic behaviors. As depicted in figure 4c. A method inspired from this work and more suitable for nonlinear restoring forces is proposed in figure 4d.

3.3 Logarithmic decrement method

Another way to assess an equivalent viscous damping is to use the so-called logarithmic decrement method. Indeed, it can be shown that, for a linear viscously damped system in free vibrations, the decreasing envelope of the displacement follows an exponential law. If the oscillator is dropped without any initial velocity, its displacement $u(t)$ is expressed in equation 7, where U_0 is the initial displacement, ξ is the viscous damping ratio and ω_0 is the natural pulsation. Two consecutive maxima of the oscillations give the logarithmic decrement δ by the equation 8 which is then useful to determine the viscous damping ratio ξ with equation 9. In the case of a non-viscous damping, the decreasing envelope is different, (e.g. it is linear for Coulomb's friction). Hence, either two different maxima have to be chosen to find the best fitting EVDR for the whole free vibrations regime, either the computation of the EVDR has to be carried out between each couple of successive maxima to determine an EVDR evolution throughout the free vibrations regime.

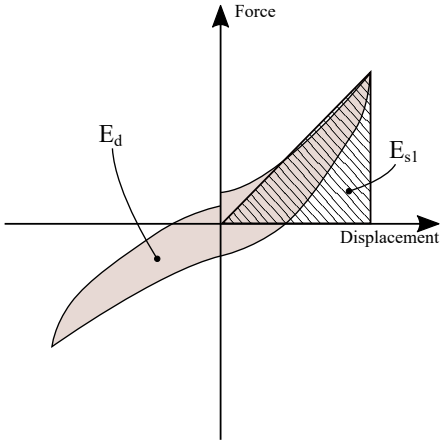

(a) Linearly stored energy evaluated on a half-cycle

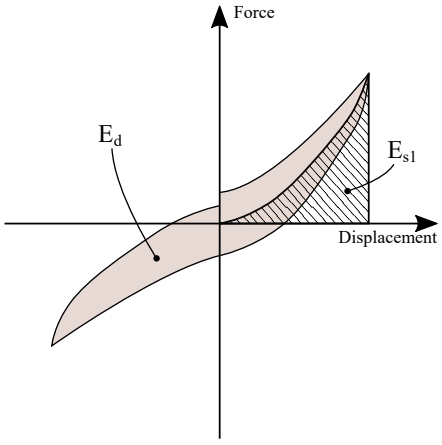

(b) Nonlinearly stored energy evaluated on a half-cycle

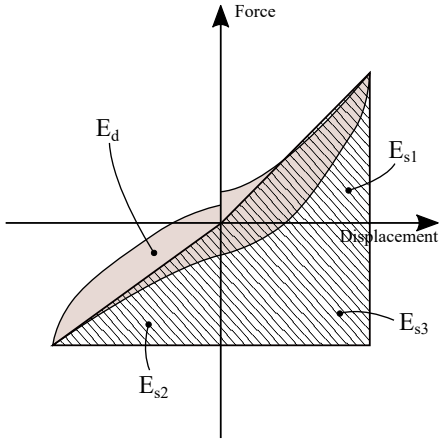

(c) Linearly stored energy evaluated on a full-cycle proposed by [18]

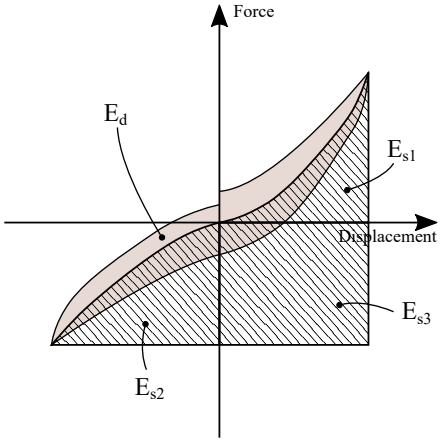

(d) Nonlinearly stored energy evaluated on a full-cycle inspired by [18]

Figure 4: Different ways to apply areas method derived from [17] and [18]

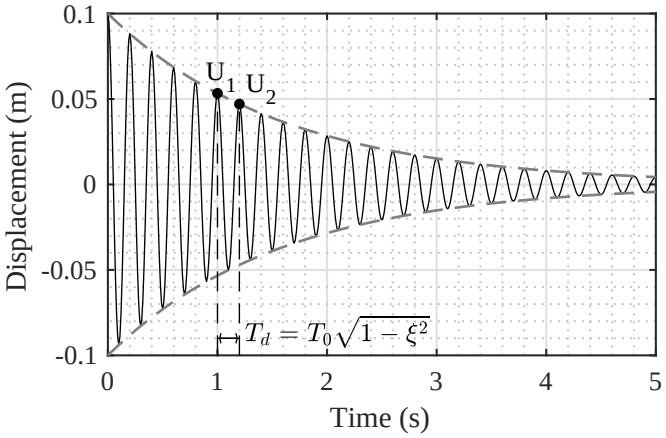

Figure 5: Logarithmic decrement principle – example with $U_0 = 0.1\,\mathrm{mm}$, $\omega_0 = 31.4\,\mathrm{rad{\cdot}s^{-1}}$ and $\xi = 2\%$

$$u(t) = U_0 \exp(-\xi\omega_0 t)\cos(\omega_0\sqrt{1-\xi^2}t) \tag{7}$$

$$\delta = \ln\left(\frac{U_1}{U_2}\right) \tag{8}$$

$$\xi = \frac{\delta}{\sqrt{4\pi^2+\delta^2}} \tag{9}$$

4 DAMPING IDENTIFICATION FROM AN EXPERIMENTAL CAMPAIGN

4.1 Quasi-static cyclic reverse test

An application of the previously described method will be presented below. A quasi-static cyclic triangular loading, labelled QSC1, is carried out thanks to 2 actuators mounted on the additional masses positions with an increasing cycle amplitude centimeter by centimeter, each cycle being repeated three times to stabilize the damage state of the beam. The time-displacement evolution of this loading is given in figure 6. In order to describe the whole response of the beam with a simple degree of freedom oscillator (SDOF), the displacement field is expressed on the first mode shape. From a theoretical point of view, the mode shape is a sinusoid modified by the presence of the additional masses (see figure 7). A full-field measurement based upon an industrial digital image correlation method has been used (VIDEOMETRIC®, [19]). This method provides displacement data all along the beam, allowing for a projection to the eigenbasis. The out-coming projection error is useful to detect nonlinearities occurring during the excitation. For a more detailed explanation of this method, please refer to [15].

The corresponding force-displacement graph is represented in figure 8, a significant pinching effect occurs. The phenomenon behind this effect is still not entirely understood. A possible explanation could be that cracks going all through the beam have a residual opening at the zero-displacement state (due for example to a misalignment between crack lips, erosion or bond slip). As a result, the inertial momentum at the crack location is reduced, since the reinforcements are the only mechanical bond between the crack lips. When bending increases, crack lips get in contact at upper or lower fiber of the beam depending on the bending direction, thus increasing again the inertial momentum of the section and consequently the bending stiffness. The model originally proposed by [20] has been modified to account for the pinching effect (which

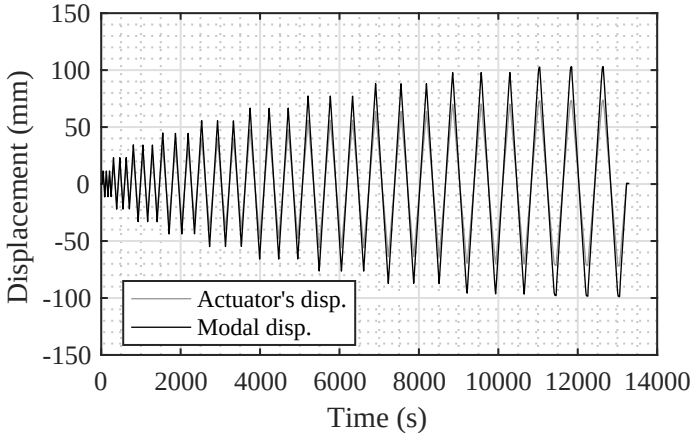

Figure 6: Imposed actuator's displacement and resulting modal displacement for the nonlinear model calibration quasi-static test

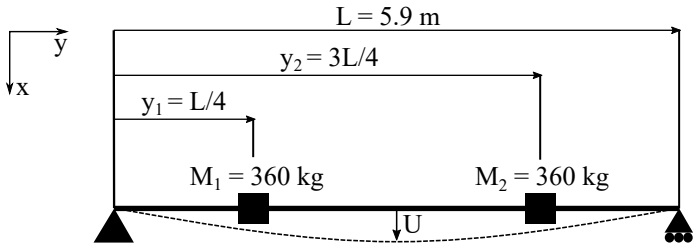

Figure 7: Simplified representation of the tests

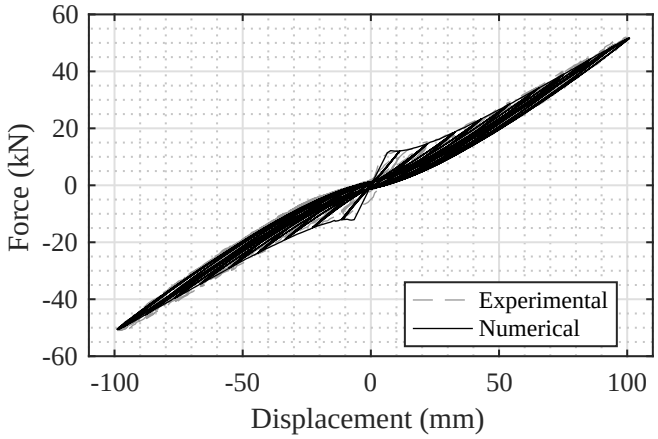

Figure 8: Force-displacement measurement for the considered QSC1 test

Name	Description	Unit
δ_y	Yield displacement	m
K_0	Initial stiffness	N.mm^{-1}
p	Stiffness loss coefficient	-
q	Fragility coefficient	-
a^π	Hysteresis loops width	N
b^π	Initial stiffness of the hysteresis loops	N.mm^{-1}
U_c	Crack closure displacement	m
l_p	Pinched stiffness coefficient	-

Table 1: Model parameters

is roughly a stiffness variation for a damaged structure when slightly deformed). Since the formulation of this model is not in the scope of this study, a simple illustration of the influence of the different parameters will be given in 4.2.

4.2 A thermodynamic-based model for bending of RC beams

Three phenomena are here modeled: damage, friction and pinching. Then, the restoring force is divided in two parts: the damage force F^p and the frictional force F^π. The constitutive law linking the force $F = F^p + F^\pi$ and the displacement u of the oscillator is ruled by the 8 parameters given in table 1. The Helmoltz's free energy Ψ and the restoring force F are expressed in equations 10 and 11.

$$\Psi = \frac{1}{2}K_0 \cdot (1 - f(u) \cdot D) \cdot (1 - D) \cdot u^2 + \frac{1}{2}K_0 \cdot D \cdot (u - u^\pi)^2 \tag{10}$$

$$F = \frac{\partial \Psi}{\partial u} = K_0 \cdot (1 - f(u) \cdot D) \cdot (1 - D) \cdot u + K \cdot D \cdot (u - u^\pi) \tag{11}$$

The stiffness loss coefficient p gives the secant stiffness for a theoretical infinite displacement while the fragility coefficient q has an influence on the initial slope of F^p-u curve when damage initiates as depicted in figure 10a. The role of both a^π and b^π in the frictional force is illustrated on figure 10b. The proposed pinching function f, expressed in equation 12 and plotted in figure 9, weights the stiffness coefficient to get a reduced stiffness depending to the displacement u and the damage level D varying between 0 and 1. In this formulation, pinching is activated only when damage exists. Hence, at the initial state, $K_p = K_0$.

$$f(u) = (1 - l_p) \cdot \exp\left(-\frac{1}{2}\left|\frac{u}{U_c}\right|\right) \tag{12}$$

$$K_p(u) = K_0 \cdot (1 - f(u) \cdot D) \tag{13}$$

4.3 Model identification

The identification process is performed by built-in methods of MATLAB®. In order to limit the risk to fall into a local minimum, the choice of a 3 steps identification has been made: (i) elastic step (δ_y, K_0), (ii) damaging step (p, q) and (iii) friction step (a^π, b^π, U_c, l_p). The error criterium to minimize is given in equation 14. For each identification step, only a part of data is used. For the elastic step, only the first displacement points prior to the elastic limit displacement δ_y are kept. Then, for the damage step, the capacity curve is deduced by keeping the

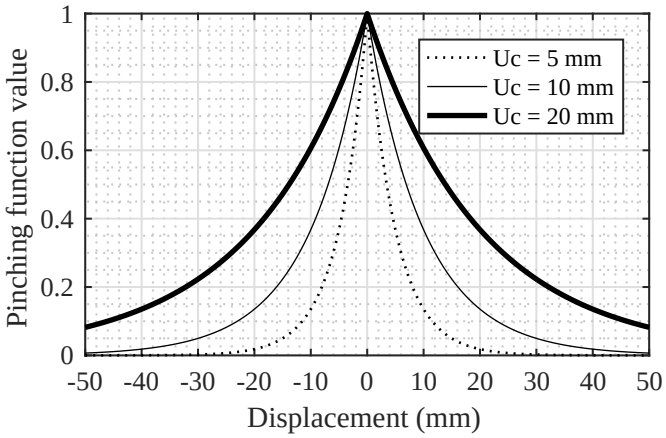

Figure 9: Plot of the pinching function over displacement (0 value corresponds to completely closed cracks)

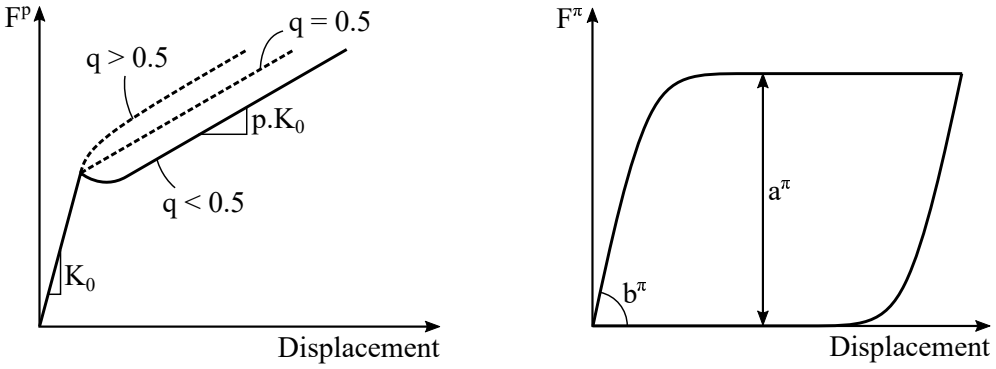

(a) Parameters influence for a monotonic loading

(b) Parameters influence for a unilateral cyclic loading (without pinching)

Figure 10: Description of some parameters influence on the model behavior

Parameter	Value
δ_y	$6.84 \times 10^{-3}\,\mathrm{m}$
K_0	$1.78 \times 10^{6}\,\mathrm{N{\cdot}m^{-1}}$
p	0.245
q	0.442
a^{π}	$1.53 \times 10^{3}\,\mathrm{N}$
b^{π}	$7.24 \times 10^{4}\,\mathrm{N{\cdot}m^{-1}}$
U_c	$5.20 \times 10^{-2}\,\mathrm{m}$
l_p	6.23×10^{-9}

Table 2: Identified parameters values

highest force value associated to each displacement from zero to maximum displacement in the time-history recording. Eventually, the friction parameters are identified within the last stabilized loop, when the dissipations do not evolve anymore and the cyclic displacement amplitude is the highest. It can be seen on figure 8 that the model identification is satisfactory.

$$\eta(t) = \frac{\int_0^t (F(\tau) - F_{exp}(\tau))^2 \cdot d\tau}{\int_0^t F_{exp}(\tau)^2 \cdot d\tau} \tag{14}$$

The identified parameters are summarized in table 2. The pinched stiffness coefficient l_p being negligible before 1, the pinching function expressed in equation 12 can be simplified to equation 15.

$$f(u) = \exp\left(-\frac{1}{2}\left|\frac{u}{U_c}\right|\right) \tag{15}$$

4.4 Equivalent viscous damping ratio evaluation using Jacobsen's method

Once the thermodynamic model presented in 4.2 is identified, it is possible to compare the EVDR obtained from different methods. The main advantage of a virtual experimental study is to avoid spurious dissipation due to external sources. Hence, the validity of the representation of hysteretic dissipation by an equivalent viscous damper is assessed.

To assess the influence of the different model's parameters and of the prescribed displacement, an increasing cyclic quasi-static displacement loading has been designed and is displayed on figure 11. Each cycle is repeated three times so the hysteretic behavior in the second and third cycle can be considered as stabilized and the energy dissipation due to damage initiation is not taken into account. It is important to note that the first three cycles are equal to the last three in order to remain at the same ductility level μ of the beam all along the loading. The definition of this ductility level is shown in equation 16, where δ_m is the maximum displacement in the time-history analysis and δ_y is the elastic limit displacement.

$$\mu = \frac{\delta_m}{\delta_y} \tag{16}$$

The dependency of the EVDR on the ductility level μ is first addressed in case of standard set of parameters given in table 2. With the identified set of parameters (line with filled black squares in figures 14a to 14f), the EVDR exhibits a strong dependency on the displacement amplitude. Starting from zero, it reaches a maximum and then decreases again asymptotically to zero (more or less quickly depending on the model parameters).

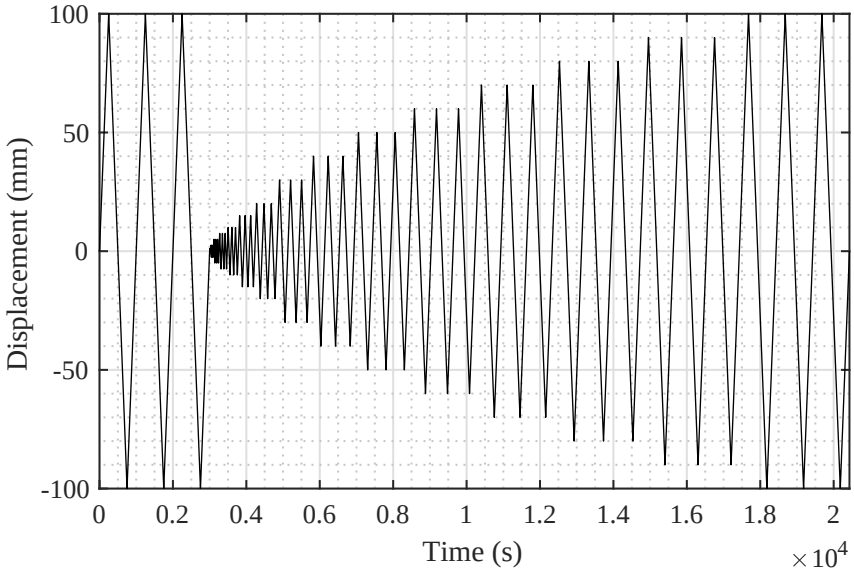

Figure 11: Loading procedure for the model's parameters sensitivity study (here for a ductility level μ = 14.6)

After, the influence of the constitutive model parameters is studied considering a constant ductility level of μ = 14.6.

4.4.1 Influence of the ductility level μ

The model including damage mechanisms, the maximum elastic energy storage decreases with the ductility level (figure 12c). The other important observation is that the dissipated energy does not seem to depend on the ductility level of structures for the present nonlinear model. However, since the equivalent viscous damping ratio depends on the ratio of the dissipated energy over the stored one, the EVDR seems to increase with respect to the ductility level (see figure 12a).

4.4.2 Influence of the hysteresis loops width a^π and slope b^π

The hysteresis loops width, driven by a^π, does not influence significantly the stored energy but highly modifies the dissipated energy per cycle E_d. When the cycles have a lower amplitude, there is an inversion of dependency between E_d and a^π because of the kinematic hardening, which explains that the EVDR is higher at low cycle displacements for lower a^π values in figure 13a.

Regarding the dissipated energy per cycle E_d, the influence of the slope of the hysteresis loops b^π fades out progressively as the latter increases. However, a lower value of b^π can make a major difference due to a drop of energy dissipation (see figure 13d).

4.4.3 Influence of the closure displacement δ_y

The pinching displacement U_c defines the domain where the stiffness is influenced by a pinching effect. As plotted on figure 14a, the equivalent viscous damping ratio is proportional to the value of U_c. Regarding the energies involved, the dissipated energy does not depend on

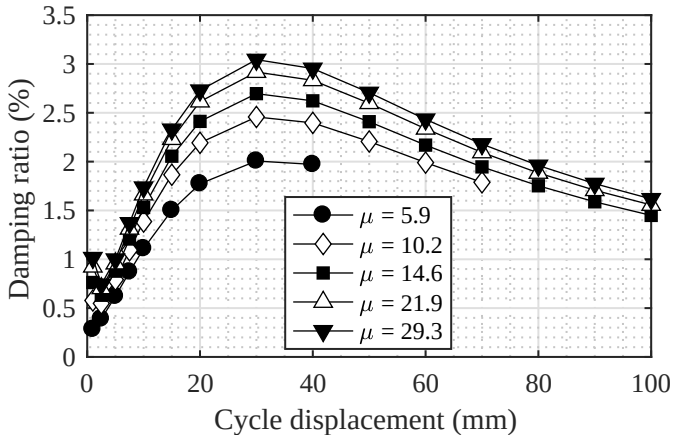

(a) Influence of the cycle amplitude on the equivalent viscous damping ξ_{eq} ratio for different ductility levels μ

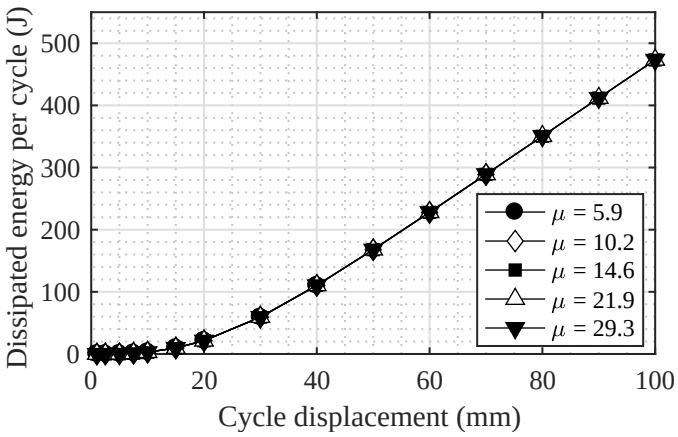

(b) Influence of the cycle amplitude on the dissipated energy E_d per cycle for different ductility levels μ

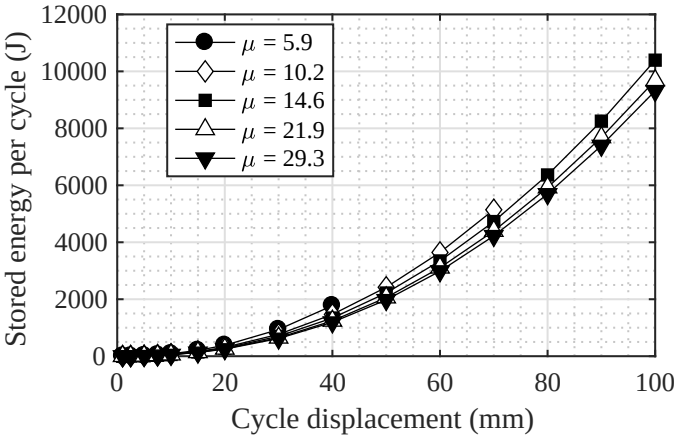

(c) Influence of the cycle amplitude on the stored energy per cycle E_s for different ductility levels μ

Figure 12: Influence of the ductility level μ over energies and equivalent viscous damping ratio ξ_{eq} for different cycle amplitudes obtained by Jacobsen's areas method

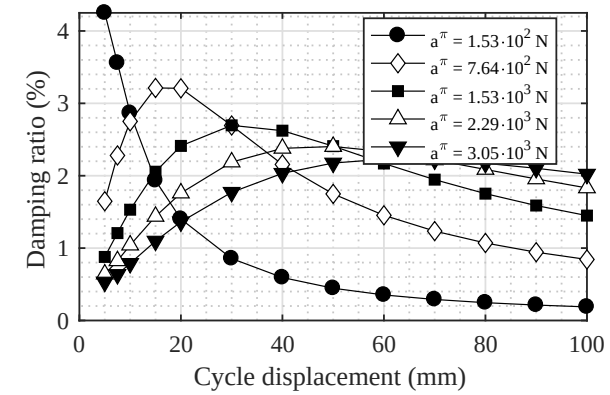

(a) EVDR ξ_{eq} for different a^π

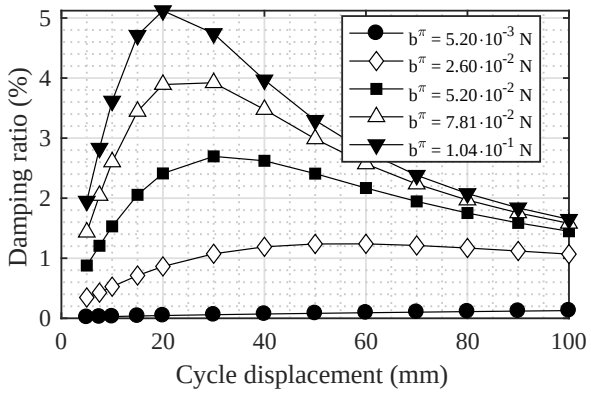

(b) EVDR ξ_{eq} for different b^π

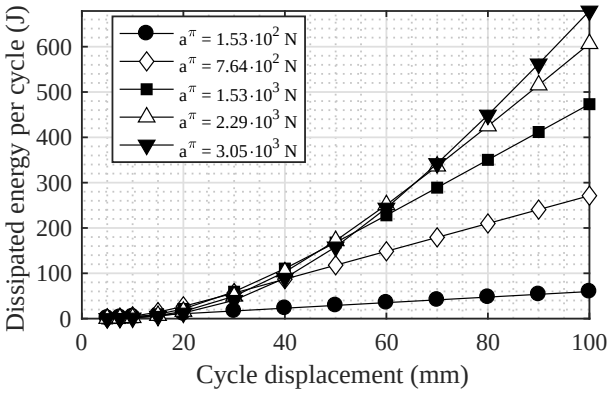

(c) Dissipated energy per cycle E_d for different a^π

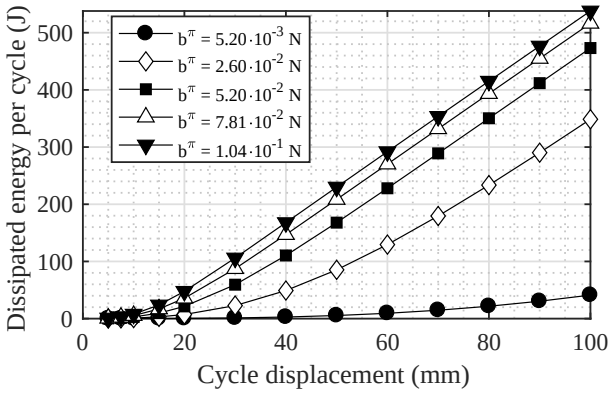

(d) Dissipated energy per cycle E_d for different b^π

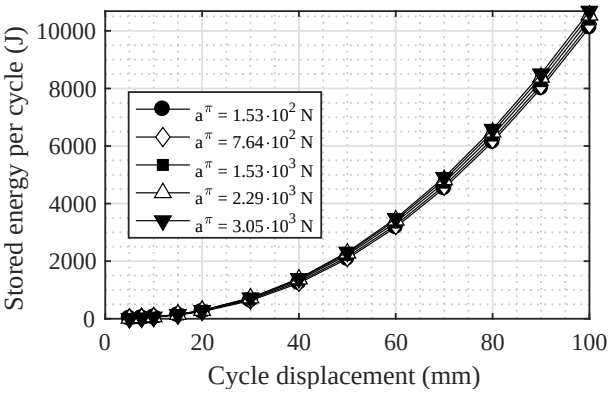

(e) Stored energy per cycle E_s for different a^π

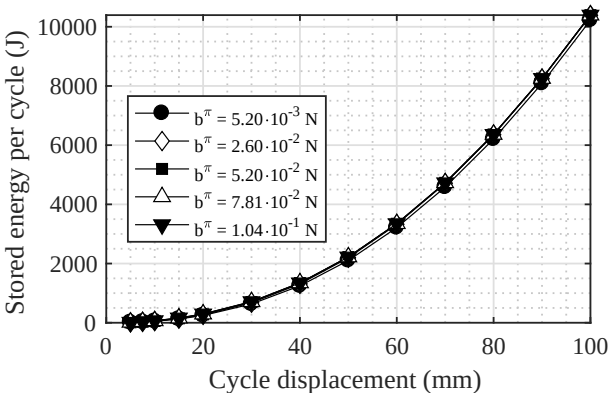

(f) Stored energy per cycle E_s for different b^π

Figure 13: Influence of the hysteresis loops width a^π and loops slope b^π over energies and equivalent viscous damping ratio ξ_{eq} for different cycle amplitudes obtained by Jacobsen's areas method

this parameter while the stored energy decreased when U_c increases. This means that the widest the pinching effect is, the less elastic energy can be stored. In agreement with the hypothesis formulated in 4.1 regarding the origin of the pinching, this would mean that, for a given constant ductility level μ, the more the residual cracks are opened (*i.e.* when no loading is applied), the more prescribed displacement it takes to store the same amount of elastic energy.

4.4.4 Influence of the fragility coefficient q

Finally, the fragility coefficient as almost no effect on the dissipated energy per cycle, but tends to lower the stored energy. Thus, the equivalent viscous damping ratio increases with the fragility coefficient (see figures 14b, 14d and 14f).

4.5 Equivalent viscous damping ratio evaluation using logarithmic decrement method

4.5.1 Loading procedure

A list of displacement levels $d_{1\leq i\leq N}$ is arbitrarily defined. The loading and post-process are performed as follows:

- a quasi-static cyclic displacement $d_{1\leq i\leq N}$ is prescribed to the oscillator in order to make it reach a given ductility level μ;
- an initial displacement d_i is prescribed to the beam;
- the beam is dropped off the initial displacement value and its free vibrations are simulated by a Newmark implicit algorithm to assess nonlinearities associated to the hysteretic model;
- the logarithmic decrement method is applied between each consecutive maxima of displacement (see figure 5);
- perform the previous steps for all i between 1 and N.

4.5.2 Comparison with Jacobsen's area method conducted in dynamics

From the different ductility levels, an EVDR is associated to a cycle amplitude of displacement and to a given period (deduced from a measured pseudo-period estimated *via* the time between the two consecutive maxima and the corresponding EVDR). The data obtained are plotted on figures 15 to 16b. The dependency of the period on the cycle amplitude seen on figure 16a is directly due to the pinching effect: the beam stiffness reduction in the neighborhood of the zero-displacement point (*i.e.* when the cycle amplitude is lower than the closure displacement U_c) is accompanied by a period increase. As shown by quasi-static tests using Jacobsen's areas method, the EVDR increases with the ductility level μ.

The value of the amplitude of displacement progressively decreases in free vibrations regime because of the energy dissipation. For each pseudo-cycle, the first maximum of displacement is considered to define the amplitude (alternatively, the second maximum or the mean of the two maxima could have been chosen). This means that for the damping value identified on the example of the figure 5, the associated displacement value would be U_1.

The values obtained for the same ductility level μ = 14.6 for both the quasi-static test described in 4.1 by Jacobsen's areas method and the present free vibration test by the logarithmic decrement method are in good agreement as depicted in figure 17. It can be argued that the areas method gives higher estimates of the EVDR than logarithmic decrement, however the relative

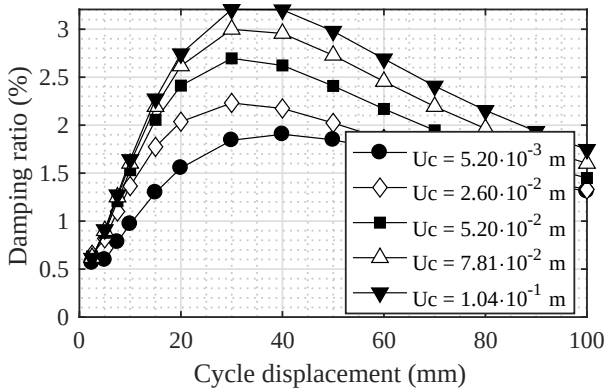

(a) Equivalent viscous damping ratio ξ_{eq} evaluated by areas method for different U_c

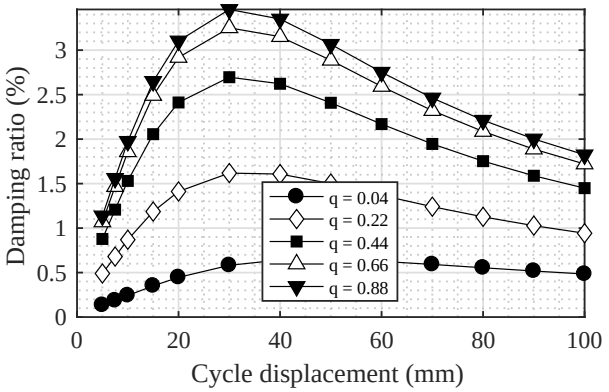

(b) Equivalent viscous damping ratio ξ_{eq} evaluated by areas method for different q

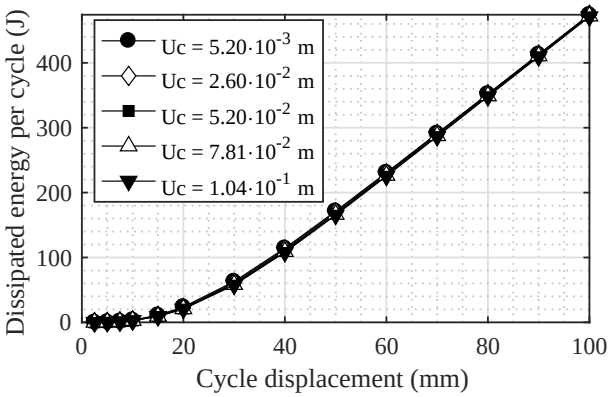

(c) Dissipated energy per cycle E_d for different for different U_c

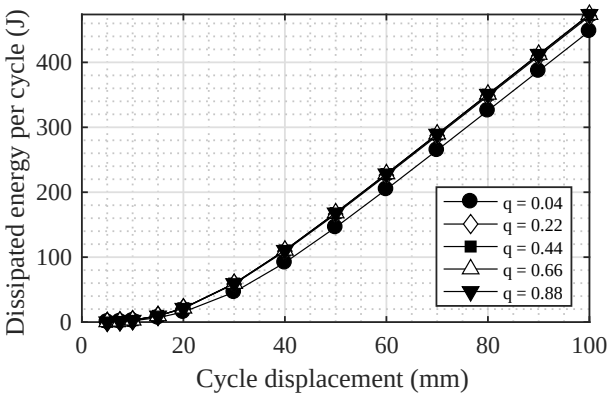

(d) Dissipated energy per cycle E_d for different q

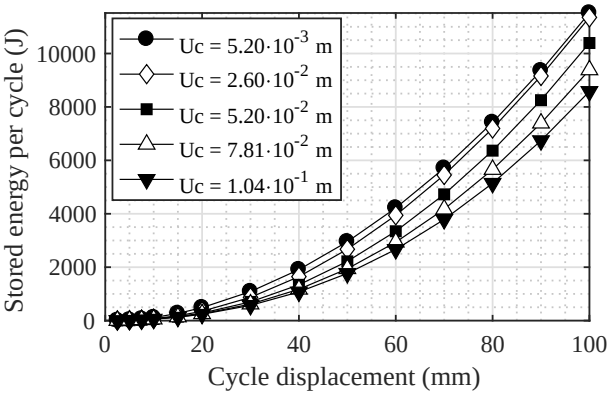

(e) Stored energy per cycle E_s for different for different U_c

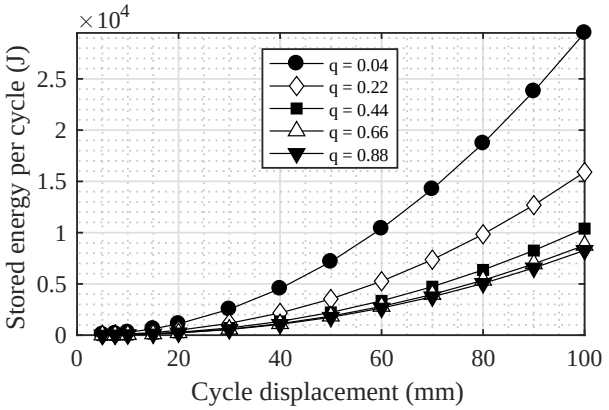

(f) Stored energy per cycle E_s for different q

Figure 14: Influence of the closure displacement U_c and the fragility coefficient q over energies and equivalent viscous damping ratio ξ_{eq} for different cycle amplitudes obtained by Jacobsen's areas method

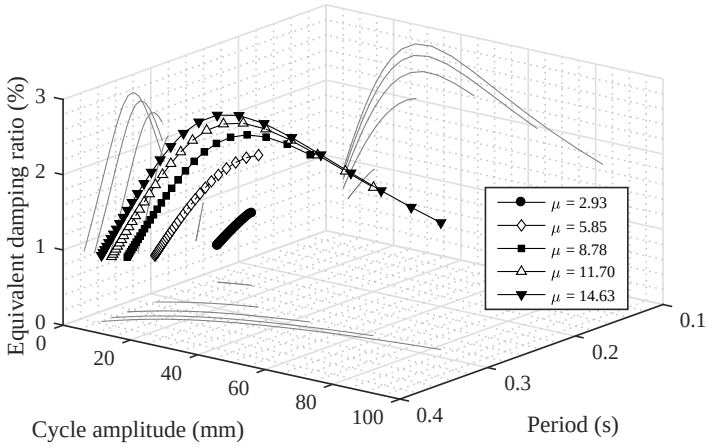

Figure 15: Equivalent viscous damping ratio *versus* cycle amplitude and measured cycle period for several ductility levels μ

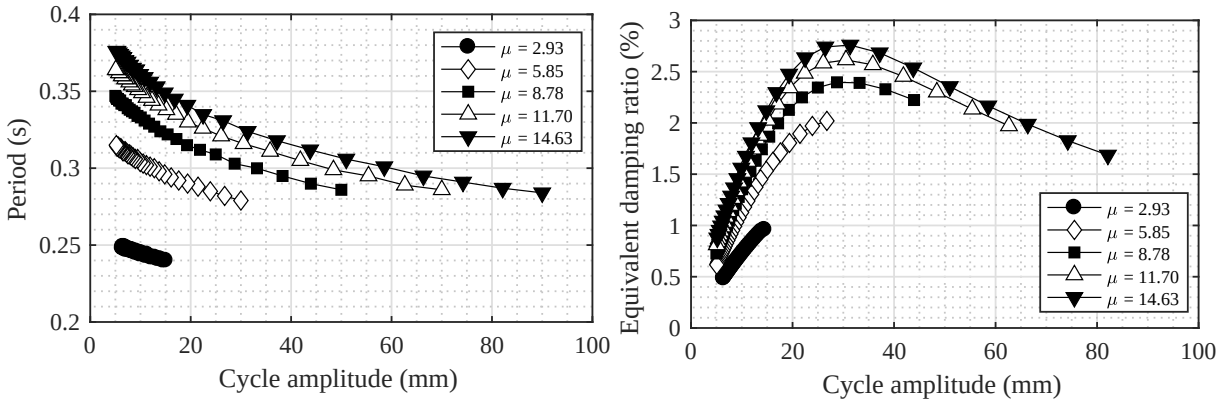

(a) Period *versus* cycle amplitude (projection of figure 15)

(b) Damping ratio *versus* cycle amplitude (projection of figure 15)

Figure 16: Influence of cycle amplitude, period and ductility level on the equivalent viscous damping ratio evaluated by the logarithmic decrement method

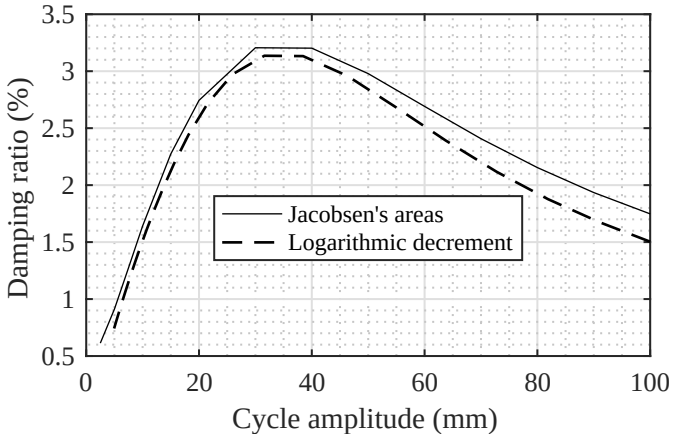

Figure 17: Comparison of the equivalent vicous damping ratio values obtained by Jacobsen's area method in quasistatic and the logarithmic decrement method in dynamics

difference remains reasonable at the maximum damping ratio (+3% of relative difference) and also in mean on the studied cycle amplitude range (+10% of relative difference).

5 CONCLUSIONS

A major experimental campaign has been carried out. In order to model the nonlinear phenomena such as pinching effect, a thermodynamic-based model has been proposed. Moreover, full-field measurements make possible the projection of beam displacements on the theoretical mode shapes which constitute an innovative post-treatment method and can be considered as a so-called "modal filter". Once the model parameters calibration has been performed through a MATLAB® built-in identification procedure, numerical simulations of quasi-static cyclic reverse tests and dynamic free vibration tests on the nonlinear oscillator associated to the beam are carried out. The comparison of the EVDR values obtained with each method did not show major differences, thus suggesting that the dynamic characteristic of the loading does not influence significantly the result, even comparing a logarithmic decrement post-treatment against Jacobsen's method. The parametric study has shown the influence of the various model parameters on the equivalent viscous damping ratio. Mostly, the ductility level and the cycle amplitude seem to have a major impact on the EVDR. Otherwise, a direct interpretation of the damping ratio as an energy dissipation indicator is a misunderstanding: the ductility level here only decreases the maximum stored energy and does not modify the energy dissipation, yet the EVDR increases with respect to the ductility level. Finally, 20 specimens have been tested either under quasi-static or dynamic loadings. Many interesting studies will be soon carried out on this experimental campaign, such as the mode combination influence on damping, velocity effects or structural and material changes influence on the dissipated energy.

ACKNOWLEDGEMENT

The authors wish to express their most grateful thanks to CEA/DEN for its financial support. The work carried out under the SINAPS@ project has benefited from French funding managed by the National Research Agency under the program Future Investments (SINAPS@ reference No. ANR-11-RSNR-0022). The work reported in this paper has also been supported by the SEISM Institute (`http://www.institut-seism.fr`).

REFERENCES

[1] F. Ragueneau, C. La Borderie, J. Mazars, Damage model for concrete-like materials coupling cracking and friction, contribution towards structural damping: first uniaxial application. *Mechanics of Cohesive-Frictional Materials*. **5**, 607–625, 2000.

[2] R. Crambuer, B. Richard, N. Ile, F. Ragueneau, Experimental characterization and modeling of energy dissipation in reinforced concrete beams subjected to cyclic loading. *Engineering Structures*, **56**, 919–934.

[3] A.A. Correia, J.P. Almeida, R. Pinho, Seismic energy dissipation in inelastic frames: understanding state-of-the-practice damping models. *Structural Engineering International*, **23(2)**, 148–158, 2013.

[4] F.A. Charney, Unintended consequences of modeling damping in structures. *Journal of Structural Engineering*, **134(4)**, 581–592, 2008.

[5] J.F. Hall, Problems encountered from the use (or misuse) of Rayleigh damping. *Earthquake Engineering & Structural Dynamics*, **35(5)**, 525–545, 2006.

[6] P. Jehel, P. Léger, A. Ibrahimbegovic, Initial versus tangent stiffness based Rayleigh damping in inelastic time history seismic analyses. *Earthquake Engineering & Structural Dynamics*, **43(3)**, 467–484, 2014.

[7] C. Cruz, E. Miranda, Evaluation of damping ratios for the seismic analysis of tall buildings. *Journal of Structural Engineering*, **143(1)**, 04016144, 2016.

[8] N. Satake, K.I. Suda, T. Arakawa, A. Sasaki, Y. Tamura, Damping evaluation using full-scale data of buildings in Japan. *Journal of Structural Engineering*, **129(4)**, 470–477, 2003.

[9] O.C. Celik, B.R. Ellingwood, Seismic fragilities for non-ductile reinforced concrete frames - Role of aleatoric and epistemic uncertainties. *Structural Safety*, **32(1)**, 1–12, 2010.

[10] T.H. Lee, K.M. Mosalam, Seismic demand sensitivity of reinforced concrete shearwall building using FOSM method. *Earthquake Engineering & Structural Dynamics*, **34(14)**, 1719–1736, 2005.

[11] Q.S. Li, K. Yang, N. Zang, C.K. Wong, A.P. Jeary, Field measurements of amplitudedependent damping in a 79storey tall building and its effects on the structural dynamic responses. *The Structural Design of Tall and Special Buildings*, **11(2)**, 129–153, 2002.

[12] K.S. Liu, Y.B. Tsai, Observed natural frequencies, damping ratios, and mode shapes of vibration of a 30-story building excited by a major earthquake and typhoon. *Earthquake Spectra*, **26(2)**, 371–397, 2010.

[13] Shaking table Azalée *Seismic Mechanic Studies Laboratory*. `http://www-tamaris.cea.fr/html/en/tests/azalee.php`. CEA Paris-Saclay, 2017.

[14] P. Jehel, A critical look into Rayleigh damping forces for seismic performance assessment of inelastic structures. *Engineering Structures*, **78**, 28–40, 2014.

[15] T. Heitz, B. Richard, C. Giry, F. Ragueneau, Damping identification and quantification experimental evidences and first numerical results. *Proceedings of the 16th World Conference on Earthquake Engineering*, paper number 1960, 2017.

[16] L.S. Jacobsen, Steady forced vibration as influenced by damping. *Transactions of ASME*, **52**, 169–181, 1930.

[17] L.S. Jacobsen, Damping in composite structures. *Proceedings of the second World Conference on Earthquake Engineering*, vol. 2, 1029–1044, 1960.

[18] S.S. Kumar, A. M. Krishna, A. Dey, Cyclic response of sand using stress controlled cyclic triaxial tests. *Proceedings of the 50th Indian Geotechnical Conference*, 2015.

[19] Videometric, `http://www.videometric.com/`. 2017.

[20] L. Moutoussamy, Real-time hybrid testing for Civil Engineering structures. *PhD Thesis Report*, École Normale Supérieure de Cachan, 2013.